Biophysical Journal Volume 66 May 1994 1489–1504

Studies on Lipid Membranes by Two-Dimensional Fourier Transform ESR: Enhancement of Resolution to Ordering and Dynamics

Richard H. Crepeau, Sunil Saxena, Sanghyuk Lee, Baldev Patyal, and Jack H. Freed
From the Baker Laboratory of Chemistry, Cornell University, Ithaca, NY 14853-1301 USA

ABSTRACT The first two-dimensional Fourier-transform electron spin resonance (2D-FT-ESR) studies of nitroxide-labeled lipids in membrane vesicles are reported. The considerable enhancement this experiment provides for extracting rotational and translational diffusion rates, as well as orientational ordering parameters by means of ESR spectroscopy, is demonstrated. The 2D spectral analysis is achieved using theoretical simulations that are fit to experiments by an efficient and automated nonlinear least squares approach. These methods are applied to dispersions of 1-palmitoyl-2oleoyl-*sn*-glycerophosphatidylcholine (POPC) model membranes utilizing spin labels 1-palmitoyl-2-(16-doxyl stearoyl)phosphatidylcholine and the 3-doxyl derivative of cholestan-3-one (CSL). Generally favorable agreement is obtained between the results obtained by 2D-FT-ESR on vesicles with the previous results on similar systems studied by continuous wave (cw) ESR on aligned samples. The precision in determining the dynamic and ordering parameters is significantly better for 2D-FT-ESR, even though the cw ESR spectra from membrane vesicles are resolved more poorly than those from well aligned samples. Some small differences in results by the two methods are discussed in terms of limitations of the methods and/or theoretical models, as well as possible differences between dynamic molecular structure in vesicles versus aligned membranes. An interesting observation with CSL/POPC, that the apparent homogeneous linewidths seem to increase in "real time," is tentatively attributed to the effects of slow director fluctuations in the membrane vesicles.

INTRODUCTION

Electron spin resonance (ESR) has played an important role in the study of membrane structure and dynamics (Freed, 1987; Marsh, 1985; Devaux and Seignenret, 1985). The high sensitivity and favorable time scale of ESR, combined with the availability of spin labels closely resembling natural membrane components, permits a detailed physical characterization of the membrane. Unfortunately, the ESR spectra arising from many biological studies are complex and can be misinterpreted if only a superficial analysis has been used. One solution to this problem is performing ESR spectroscopy on macroscopically aligned samples, which provides enhanced spectral resolution and orientation dependence. Then careful spectral simulation enables one to quantify the details of membrane structure and dynamics and how they change as a function of membrane composition and temperature (Kar et al., 1985; Tanaka and Freed, 1984, 1985). However, for many biologically relevant systems it may not be conveniently possible to prepare macroscopically aligned samples, whereas macroscopically disordered "dispersion" samples containing spin-labeled molecules may readily be prepared. But the superposition of spectra from membrane fragments that are randomly oriented greatly reduces the spectral resolution by analogy to the loss in resolution in x-ray studies on powders versus single crystals. This loss in resolution is a major source of ambiguity in the analysis of the ESR spectra, to which we refer as MOMD (i.e., microscopically ordered but macroscopically disordered) ESR spectra (Meirovitch et al., 1984; Ge and Freed, 1993).

Received for publication 26 October 1993 and in final form 13 December 1993.

0006-3495/94/05/1489/16 $2.00

Another cause of the rather low resolution is the preponderant use of continous wave (cw) ESR spectra, which suffers from significant inhomogeneous broadening, due to proton superhyperfine structure (shfs). This inhomogeneous broadening masks the sensitivity to the homogeneous linebroadening resulting from the motional dynamics even for well aligned samples. In the macroscopically disordered "dispersions" the MOMD effect provides considerable inhomogeneous broadening that further masks the sensitivity to dynamics. In principle, this MOMD effect on the linewidths and lineshapes, and how it varies with hyperfine (hf) line, can be utilized to obtain information on the ordering, but it is difficult to deconvolute from the effects of proton shfs as well as broadening from the motional dynamics, even with valiant attempts at detailed spectral simulation (Ge and Freed, 1993).

TWO-DIMENSIONAL FOURIER TRANSFORM ESR

Our group has been working intensively during the past several years to develop the new two-dimensional Fourier-transform electron spin resonance (2D-FT-ESR) techniques to supply the needed resolution (Gorcester and Freed, 1988; Gorcester et al., 1989a; Gorcester et al., 1990; Lee et al., 1993). In this paper, we wish to report our success in the study of membrane vesicles containing standard spin-labeled lipids and labeled cholesterol. In simple terms, the extra spectral dimension may be utilized to provide the enhanced resolution. However, this does not adequately convey the richness of detail provided by these new techniques.

To appreciate this, we first distinguish two types of 2D-FT-ESR experiments (Gorcester et al., 1990). The first are the two-pulse experiments of COSY (correlation spectroscopy) ESR (cf. Fig. 1*c*) and the related SECSY (spin-echo

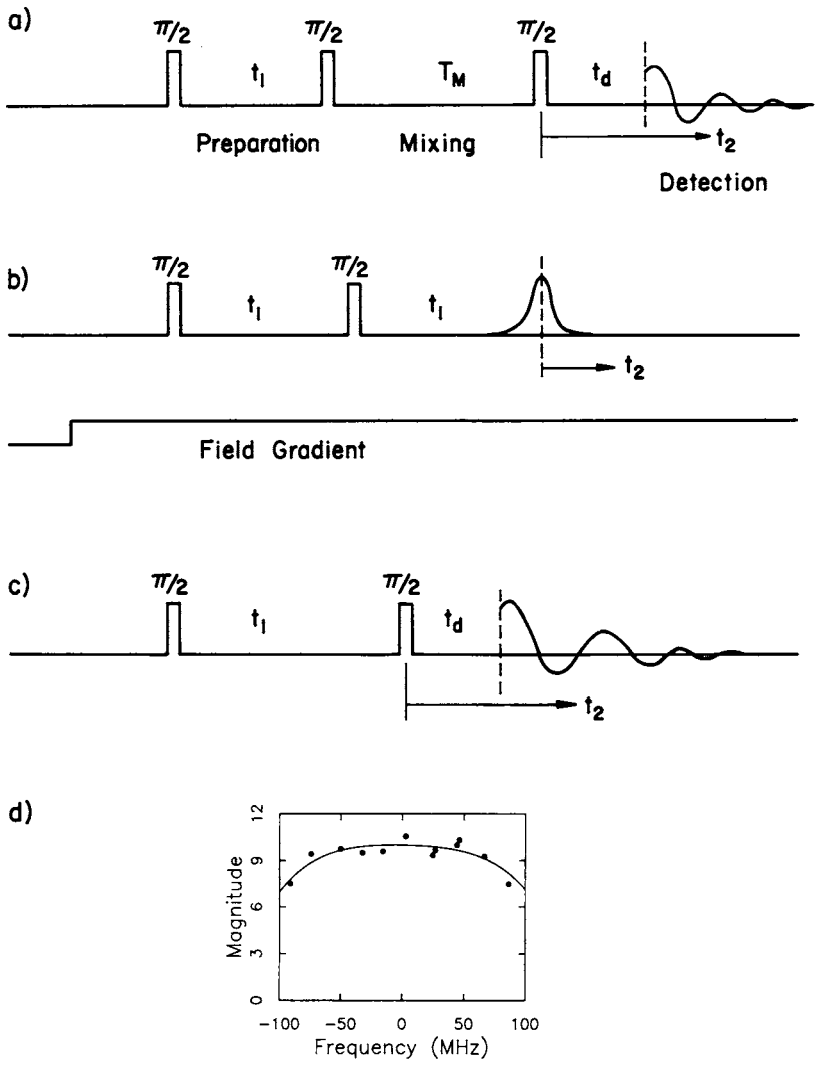

FIGURE 1 The pulse sequences used for the 2D ESR experiments. (*a*) ELDOR; (*b*) SECSY; and (*c*) COSY pulse sequences. The insert (*d*) shows the signal height of the central hf line of the magnitude Fourier transform (in arbitrary units) of a single pulse FID collected for different dc-magnetic field values, which are plotted as a function of frequency offset from the Larmour frequency. The smooth curve represents a typical coverage correction function $C(f_2)$ used for a 16PC/POPC sample.

correlation spectroscopy) ESR (cf. Fig. 1*b*), and the second are the three-pulse experiments, especially 2D ELDOR (electron-electron double resonance) (cf. Fig. 1*a*). In the first class, SECSY ESR has the advantage of spin-echo spectroscopy by providing the homogeneous linewidths (hence the T_2 values) across the inhomogeneously broadened ESR spectrum from which to infer motional dynamics. We have found that equivalent, as well as additional information may be obtained from the COSY ESR. A characteristic of COSY ESR, that is shared by all 2D-FT-ESR experiments based on collection of free-induction decays (FIDs), is that one detects a dual quadrature signal, i.e., a signal which is complex (with a real absorptive part and an imaginary dispersive part) with respect to each of the two frequencies characterizing the 2D experiment (Gorcester et al., 1990). Appropriate linear combinations provide, first of all, an ordinary complex 2D signal that is FID-like, because it is not refocused by the second pulse (it is called the S_{c+} signal). The other complex 2D signal that is obtained is echo-like, because it is refocused by the second pulse (it is the S_{c-} signal) (Gamliel and Freed, 1990). In the absence of inhomogeneous broadening the two are identical. In the presence of inhomogeneous broadening the S_{c-} and S_{c+} signals are substantially different: the S_{c-} 2D spectra are substantially sharper due to an echo-like cancellation of the inhomogeneities, which does not occur for the S_{c+} spectra. Thus a comparison of the S_{c-} and S_{c+} signals will provide useful information to distinguish homogeneous from inhomogeneous broadening, and the variation of the inhomogeneous broadening with hf line provides direct information on the MOMD contribution.

Even more detailed information providing more precise distinctions emerges from the 2D ELDOR experiment (Gorcester et al., 1990). In this experiment, off-diagonal, or cross-peaks appear which are a measure of the magnetization transfer by spin-relaxation processes during the mixing time, T_m. These cross-peaks are frequency discriminated from the auto or diagonal peaks (i.e., the ones that are observed in the COSY ESR experiment). The principal spin-relaxation mechanisms are the intramolecular electron-nuclear dipolar (END) interactions, which lead to nuclear spin-flip transitions (with rate W_n) that report on the rate of rotational reorientation, and the Heisenberg exchange (HE) rate, which reports on the bimolecular collision rate of the spin-labeled molecules. The pattern of cross-peaks enables one to dis-

tinguish the contributions from each relaxation mechanism. It is useful to obtain a series of spectra for different mixing time, T_m, to observe how these cross-peaks "grow-in" relative to the auto peaks as a result of these cross-relaxation mechanisms. With this additional time variable, one is performing a three-dimensional (3D) experiment.

In the case of MOMD spectra from membrane vesicles, we find an important role for the inhomogeneous broadening. We find that in 2D ELDOR it is now possible to utilize the different shapes of the auto peaks and the cross-peaks to precisely distinguish the contribution to broadening from the proton shfs, which is the same for each hf line, and the MOMD effect, which differs for each hf line as we have noted. Again the effects are different for the S_{c-} and S_{c+} complex signals from the 2D ELDOR. For the S_{c-} signal there is an echo-like cancellation for the auto peaks, but the cross-peaks that develop have a new feature. During the evolution period (given by t_1) a given spin label belonging to hf component "a" will evolve with the inhomogeneity associated with this hf component. After it exchanges to hf component "b" during the mixing time, T_m, it will evolve with the refocused inhomogeneity during the detection period (given by t_2). If the inhomogeneities associated with hf components "a" and "b" are different, as is the case of the MOMD contribution, but not for the contribution from proton shfs, then their differences will show up in the cross-peak broadenings. The cross-peak shapes compared with the auto peak shapes therefore provide a sensitive measure of the MOMD inhomogeneity effects and hence the extent of the ordering. In the case of the S_{c+} 2D spectra, these inhomogeneities are additive for the cross-peaks as for the auto peaks, thereby supplying supplementary information on the MOMD effect.

Given the subtle interplay of the various relaxation processes on the cross-peak intensities and the homogeneous linewidths, and of the various sources of inhomogeneous lineshape on the auto and cross peaks, we find that the most effective way of extracting the relevant relaxation and ordering data is to perform nonlinear least squares (NLLS) fitting of the 2D spectral simulations to the experiments. The detailed theory for simulating 2D-FT-ESR spectra is described elsewhere (Lee et al., manuscript in preparation). The NLLS fitting of the 2D spectra is analogous to our methods for fitting cw ESR spectra from oriented multilayers, but is much more sophisticated. Aside from the more complex theory, we simultaneously fit the full 3D data set (i.e., the set of 2D spectra, both S_{c-} and S_{c+}, obtained for the different mixing times, T_m). We show in this paper that such experiments enable us to determine ordering and dynamic parameters from vesicles at least as accurately as previously obtained from cw ESR on oriented multilayers.

MATERIALS AND METHODS

Materials

1-Palmitoyl-2-oleoyl-*sn*-glycerophosphatidylcholine (POPC) was purchased from Avanti Polar Lipid Inc., Birmingham, AL, and was used without further purification. The spin probe 1-palmitoyl-2-(16-doxyl stearoyl)-phosphatidylcholine (16PC) was a gift from Professor G. W. Feigenson, Department of Biochemistry, Cornell University, who synthesized it according to standard methods (Hubbell and McConnell, 1971). The 3-doxyl derivative of cholestan-3-one (CSL) was purchased from Syva Co., Palo Alto, CA.

Sample preparation

16PC samples

A measured amount of 1 mM 16PC in chloroform stock solution was added to 70 mg of POPC in excess chloroform to yield 1 mol %. The solution was dried under flowing nitrogen and a small excess of water was added to form a saturated dispersion. The mixture was transferred to a thin-walled TPX sample cell (Popp and Hyde, 1981) designed to provide gas exchange through the semipermeable material and to fit in our bridged loop-gap resonator (Gorcester et al., 1990). Humid nitrogen gas was used for the temperature control during data collection, and this also served to remove any dissolved oxygen that could lead to spectral broadening.

CSL samples

A measured amount (0.346 ml) of 1.9 mM CSL in chloroform stock solution was added to 50 mg of POPC (in excess chloroform) to yield a 1 mol % concentration of the spin probe. The sample was contained in a 3-mm-outside diameter glass tube. The chloroform was removed by desiccating on the vacuum line for about 24 h, and a small excess of water was added to form a saturated dispersion. The sample was then degassed to a pressure of approximately 1×10^{-4} torr and sealed. In our experience this second method of preparation proved to be more convenient for the 2D-FT-ESR experiments.

2D-FT-ESR experiments

The pulsed ESR spectrometer used in these experiments is described elsewhere (Gorcester and Freed, 1988; Gorcester et al., 1990; Lee et al., 1993) and we mention here only key features for these experiments.

We used three $\pi/2$ pulses with width of 4–5 ns for the ELDOR experiments (cf. Fig. 1*a*). The pulse widths for each set of experiments were determined so as to maximize the FID from a single pulse. It should be noted that a nominal 5 ns $\pi/2$ square pulse (corresponding to 17.9 G microwave magnetic field in the rotating frame) is predicted to provide nearly uniform spectral rotation over a ± 50 MHz bandwidth, and for magnitude spectra the "half-amplitude response" bandwidth is ± 135 MHz (Hornak and Freed, 1986; Gorcester and Freed, 1988; Gorcester et al., 1990). However the actual pulse shapes deviate from simple square pulses (Crepeau et al., 1989), so the actual coverage across the whole spectrum from a single $\pi/2$ pulse was carefully measured as described by Crepeau et al. (1989) to provide the spectrometer coverage correction factor to the magnitude spectra for each set of experiments, as discussed in the next subsection. A typical coverage profile is shown in Fig. 1*d*.

We collected the FID signal with a spectrometer dead time, t_d of 67 ns for the 16PC sample and 75 ns for the CSL sample after the third pulse in the ELDOR experiments. The separation between the first two pulses, t_1, was stepped with 128 steps of 3 ns from an initial value of 50 ns or 60 ns depending on the signal strength and other factors. The FID was collected as a function of t_2 for a total of 256 complex points with an effective step size of 1 ns. This was achieved by automatically interleaving five separate collections, each sampled with 5-ns steps using our two-channel DSP signal averager. These individual collections were offset from 0 to 4 ns relative to the microwave pulses by stepping the trigger to our custom-made, 200-MHz coherent digital clock which provides the timing for the DSP signal averagers (Lee et al., 1993). Sixty-four points were collected for each of these intermediate collections, and the signals were interleaved in the DEC 11/73 computer. A 32-step dual quadrature phase cycling sequence modified from the 16-step sequence of Gamliel and Freed (1990) provided for subtraction of all unwanted signals like the image peaks, transverse signals, and axial peaks. The additional 16 steps provide further elimination of instrumental artifacts that were not fully removed by the original 16-step phase

sequence. A full data collection at one t_1 point consisted of 500 averages for each of the 32-phase-cycle steps repeated for each of the five interleaved collections. Repeating this for 128 t_1 steps required about 20 min at the 10-kHz repetition rate for the three-pulse ELDOR sequence. The full dual quadrature signal was collected, so that later analysis of both the S_{c-} and S_{c+} components (Gamliel and Freed, 1990) could be conducted. The experiments were repeated for a series of mixing times, T_m, ranging from 74 ns to 3 μs. Results were obtained at several different temperatures.

Fig. 1*b* is the two-pulse sequence used in the SECSY data collections that were performed for 16PC. Two $\pi/2$ pulses were used with spectrometer dead times similar to those given above, and the echo signal was collected starting at its peak, with 1-ns steps by interleaving in t_2 as described above. An applied magnetic field gradient damped out the FID signals and sharpened the echo signal. The pulse separation t_1 was incremented by 5-ns steps starting at 100 ns for 128 steps.

Figure 1*c* is the two-pulse sequence used in the COSY data collections that were performed for CSL. Here the FID was collected after a 62-ns dead time, and the stepping in t_1 and t_2 was performed exactly as for the 2D ELDOR experiment. For the COSY and SECSY experiments a 16-pulse sequence (Gamliel and Freed, 1990) was used to eliminate unwanted terms.

Data processing

With the improvement of instrumental dead times in t_1 and t_2 we found it necessary to correct for some instrumental artifacts that arose for the small values of t_1 in the SECSY, COSY, and ELDOR results. The first two microwave pulses showed an interaction as a function of their separation up to about 200 ns resulting in a slight width and phase variation of the second pulse. Additionally, for very short t_2 values and longer values of t_1, we observed what seemed to be incomplete cancellation of the FID signal from the third pulse resulting in occasional large spikes in that region of the data collection. The first of these effects caused a multiplication of the error-free data by a complex function of t_1 and was eliminated by determining an instrument response function as follows. A 2D ELDOR (or SECSY ESR or COSY ESR) experiment was performed on a reference sample known to give a sharp Lorentzian line shape in f_1 (either perdeuterated tempone in toluene or a crystal of lithium phthalocyanine was used). The resulting data set, after discarding the region of data corrupted by noise in t_1 (i.e., <200 ns), was fit by linear prediction (Gorcester et al., 1990), and only those frequencies known to be caused by the ESR signal itself were retained. This process was simple because the noise tended to cluster in peaks separated along f_1 from the signal peaks. The Lorentzians due to the signal were then used to calculate a corrected time domain data set as a function of t_1 at the specific value of f_2 corresponding to the main peak of the 2D frequency domain data, and then a complex filter function $F(t_1)$ was calculated as $F(t_1) = S(t_1)/M(t_1)$, where $S(t_1)$ is the filtered data and $M(t_1)$ is the measured data. All quantities are complex, and for large t_1, $F(t_1)$ approaches 1.0. A single reference collection was found to be sufficient for various values of T_m in the ELDOR collection and for a wide range of temperatures, because the origin of the spectral distortions is largely in the microwave pulses. Results presented in this paper are all treated in this manner.

After correction for the instrument response function, a further filtering was applied to remove any spike noise noted above, for some of the 16PC data; it was not needed for the CSL data. To identify the noise spikes, each data set was Fourier-transformed in two dimensions, and frequency filtered to restrict the frequencies to the expected three lines of the spectrum (which cover a total of approximately 100 MHz) as determined by the central field and microwave frequency of each experiment. An inverse transform represented the ESR signal well but no longer had the spike noise (which was high frequency) in the original data. A comparison of each row, t_1, or column, t_2, of the smoothed versus the original data then identified the spike noise we wanted to eliminate. The identified noise (difference greater than 4 or 5 SD) of each row or column was then replaced by the value of the filtered data set at the corresponding point. This procedure was generally quite successful in minimizing the occasional spikes (<1% of the data points) in the full data set.

In preparation for the nonlinear least squares fitting of the data to the theoretical simulations, a double Fourier transform of the data set was calculated. The magnitude spectrum was used to avoid having to make corrections for phase variations across the 2D ESR spectrum, which result from the finite dead times and the use of microwave magnetic fields of finite strength (Gorcester and Freed, 1988; Gorcester et al., 1990; Patyal et al., 1990; Lee et al., 1993). This was performed for both the S_{c-} and S_{c+} combinations of the dual quadrature data. These spectra were then corrected for the spectrometer coverage (noted above) that was determined from a set of single-pulse FID data collections for a range of different magnetic field values to cover the whole spectrum (cf. Fig. 1*d*). The coverage was expressed as a function $C(f_2)$, varying from 1.0 near the center frequency and decreasing for higher or lower frequencies. Typically it was no lower than 0.85–0.9 at the outer frequencies. For the two-pulse SECSY and COSY (and the three-pulse ELDOR experiments), the first (and second) pulses were also corrected for coverage using this function as $C(f_2)$. (In utilizing the same function to correct the coverage of the first two pulses, we are assuming that the dominant reason for imperfect coverage is the finite magnitude of the microwave magnetic field in the pulse. The observed FID signal actually has an additional correction to coverage due to the finite bandwidth of our ($Q \approx 40$) loop-gap resonator, but we found no significant change in our results when we approximately corrected for this).

Nonlinear Least Squares Simulations

The spectra were analyzed to obtain the ordering, rotational, and translational dynamics using the 2D-FT-ESR spectral simulation theory and computer programs of Lee et al. (manuscript in preparation) which are based on the stochastic-Liouville theory for time domain ESR that has been reviewed by Schneider and Freed (1989). The fitting of the experiment by the theory was performed using a NLLS procedure, analogous to those utilized for cw ESR (Crepeau et al., 1987; Shin and Freed, 1989), to obtain the optimum parameters, which we describe below.

The rotational mobility of the spin-labeled molecules is characterized by the rotational diffusion constants, $R_\perp$ and $R_\parallel$, which represent the principal values of an axially symmetric rotational diffusion tensor. For 16PC and CSL they represent motion parallel and perpendicular to the preferred orientation of the long-hydrocarbon chain, and the long molecular axis, respectively. For 16PC they represent a simple approximation to the complex internal modes of motion of the chain as well as the overall motion (Ferrarini et al., 1989). The translational mobility is characterized by the frequency of Heisenberg exchange (ω_{HE}), which measures the rate of bimolecular encounters of the spin-labeled molecules.

The lipid and cholesterol molecules in the bilayers experience ordering potentials, which restrict the amplitudes of the rotational motion. That is, the larger the ordering potential, the smaller will be the range of orientations sampled by the motion. This potential, $U(\Omega)$, determines the orientational distribution of the molecules with respect to the local ordering axis of the membrane bilayer, known as the local director (corresponding to each bilayer segment in the vesicle). It is usually expressed as an expansion in generalized spherical harmonics,

$$-U/kT = \epsilon_0^2 \mathscr{D}_{00}^2(\Omega) + \epsilon_2^2(\mathscr{D}_{02}^2(\Omega) + \mathscr{D}_{0-2}^2(\Omega)) + \epsilon_0^4 \mathscr{D}_{00}^4(\Omega) + \cdots$$

where $\Omega = (\alpha, \beta, \gamma)$ are the Euler angles between the molecular frame of the rotational diffusion tensor and the local director frame. The ϵ_0^2, ϵ_2^2, and ϵ_0^4 are dimensionless potential energy coefficients. Also k is Boltzmann's constant, and T is the temperature. The commonly used order parameter S, is defined by

$$S = \langle \mathscr{D}_{00}^2 \rangle = \left\langle \frac{1}{2}(3\cos^2\beta - 1) \right\rangle = \frac{\int d\Omega \exp(-U/kT)\mathscr{D}_{00}^2}{\int d\Omega \exp(-U/kT)}$$

and another order parameter $S_2 = \langle \mathscr{D}_{02}^2 + \mathscr{D}_{0-2}^2 \rangle$ is defined in a similar manner. It represents the deviation from cylindrical symmetry of the molecular alignment relative to the local director.

For simulating the spectra from lipid vesicles the MOMD model was incorporated. This means that the different bilayer segments are randomly oriented with respect to the lab z axis defined as the axis of the static-magnetic field. We therefore calculated spectra for 20 different values of Ψ, for CSL, (and 10 different values of Ψ for 16PC), and averaged them on the unit sphere to produce a single MOMD spectrum. Here Ψ is the angle between the local director and the dc-magnetic field.

The values of the magnetic tensor $\bar{A}$ used were $A_x = A_y = 4.9$ G, $A_z = 33.0$ G for 16PC, and $A_x = 5.6, A_y = 5.3, A_z = 33.8$ G for CSL (Shin and Freed, 1989). For the g-tensor we used $g_x = 2.0089$, $g_y = 2.0058$, $g_z = 2.0021$ for 16PC and $g_x = 2.0081$, $g_y = 2.0061$, $g_z = 2.0024$ for CSL (Shin and Freed, 1989).

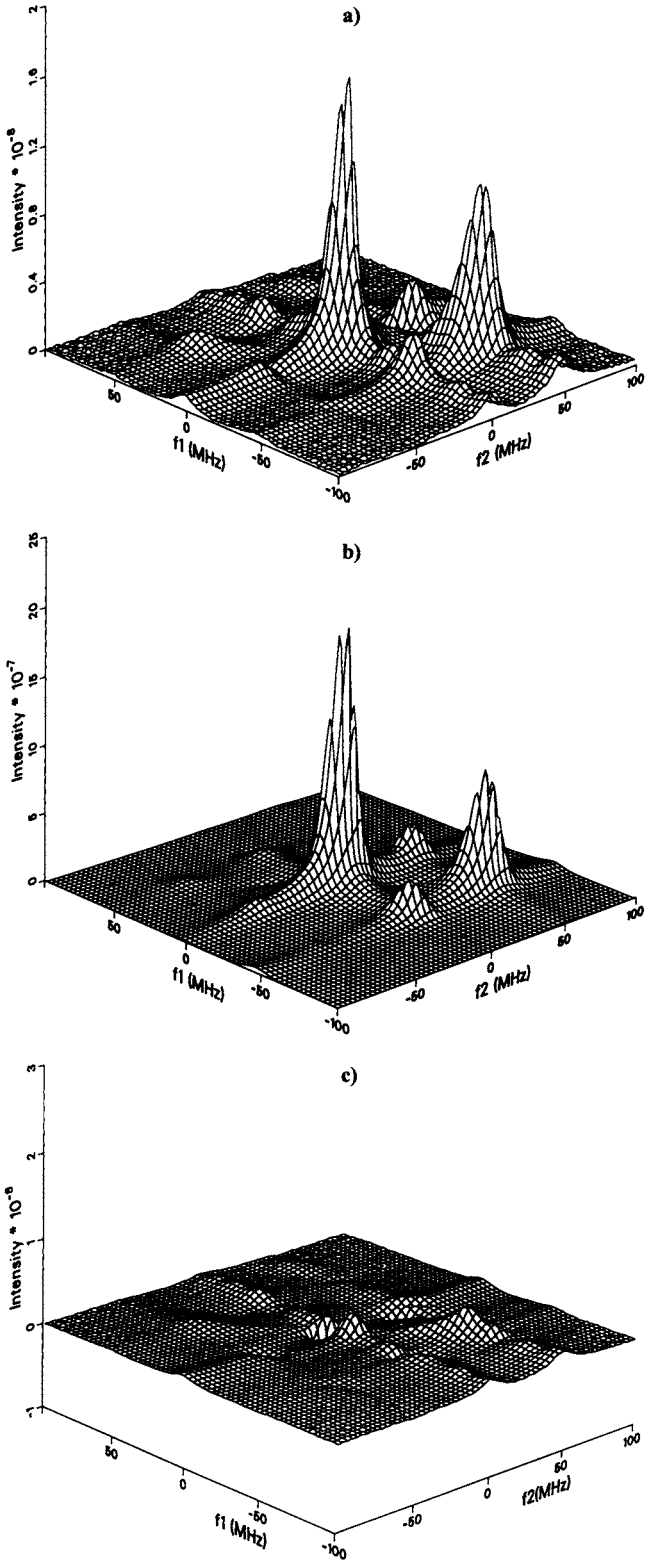

FIGURE 2 Plots of (*a*) experimental, (*b*) best NLLS simulation, and (*c*) the difference between *a* and *b* for a 2D ELDOR spectrum from CSL/POPC.

Additional fitting parameters included a Gaussian inhomogeneous width parameter Δ, as well as a Lorentzian homogeneous width contribution T_{2e}^{-1}, representing additional broadening mechanisms (see Results and Discussion). The simulations also include the effect of the dead times in t_1 and t_2 which were fixed at the experimentally measured values. The effect of the finite pulse widths was approximated by measuring t_1, t_2, and T_m from the midpoints of each pulse. For t_1 and t_2 this may be regarded as a small correction to the dead time (i.e., 4–5-ns pulse widths vs 50–75-ns dead times). (The theoretical analysis of our experiments showed that the spectral modes that determine the spectrum exhibited decay constants (i.e., effective T_2 values) of approximately 50–100 ns, which are long compared to the pulse widths.)

The first step of the NLLS simulation was to choose reasonable starting values for ϵ_0^2, ϵ_2^2, ϵ_0^4, $R_\parallel$, $R_\perp$, and ω_{HE}. The fitting procedure consisted of several iterations by a Marquardt-Levenberg algorithm that was accelerated by the inclusion of the "trust-region" algorithm (More, 1977) until a minimum in the least squares was achieved. We simultaneously fit the set of 2D ELDOR spectra obtained for a series of mixing times, T_m, as well as both the S_{c-} and S_{c+} spectra when available, to obtain the optimum parameters. In fitting a set of 2D spectra with different mixing times, the electron spin relaxation rate, W_e, is also determined implicitly. Note that the COSY-ESR experiment is formally equivalent to the 2D ELDOR experiment with $T_m = 0$; so in the case of the CSL study, both 2D ELDOR and COSY ESR were fit simultaneously. The quality of the overall fit to experiment that we are able to obtain is illustrated in Fig. 2 where we show the difference between a typical experiment and the NLLS fit.

RESULTS AND DISCUSSION

General features

Experiments were performed initially on 16PC samples to serve as a test in developing and demonstrating the potential of the FT ESR experiments on lipid vesicle dispersions. A typical time domain representation of one of the quadrature components of the collected ELDOR signal corresponding to the sum $S_{c-} + S_{c+}$ is shown in Fig. 3. The rapid decay in the t_2 and t_1 directions is the major experimental challenge, because the signal is approaching the noise level after about

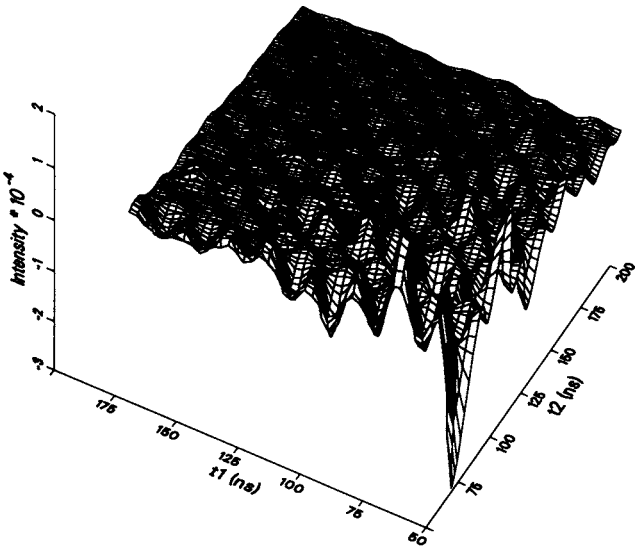

FIGURE 3 Time domain representation of the observed ELDOR experiments for 16PC/POPC at 45°C with a mixing time, T_m, of 600 ns. This is a stack plot of one of the quadrature components corresponding to $S_{c-} + S_{c+}$.

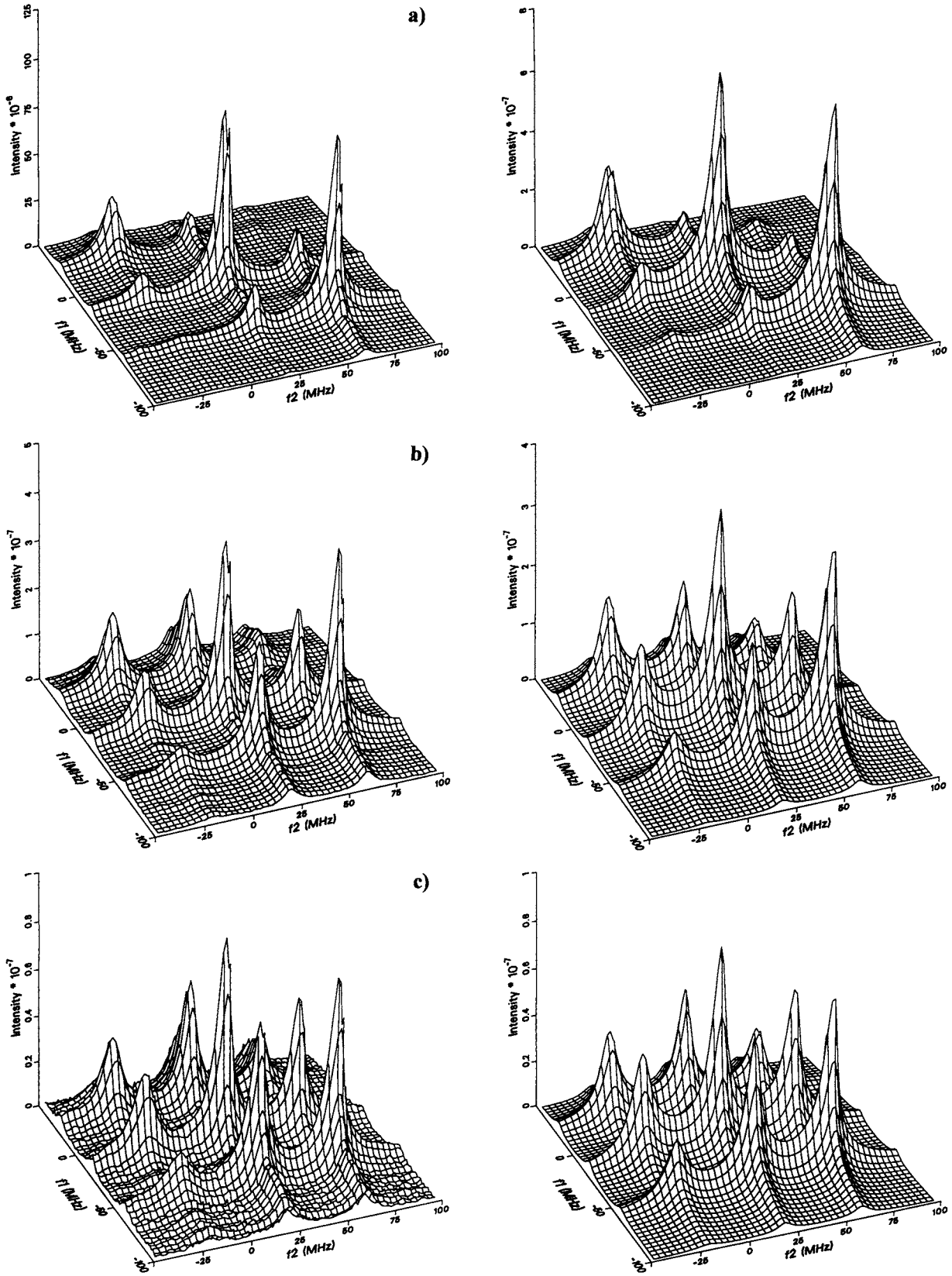

FIGURE 4 2D ELDOR experiments (*left side*) and simulations (*right side*) for 16PC/POPC at 45°C as a function of mixing time, T_m. (*a*) 200 ns; (*b*) 600 ns; and (*c*) 1200 ns. The S_{c-} signal is shown.

200 ns. In fact for CSL/POPC data collections with the much shorter decays, the S_{c+} signal decayed too quickly for us to detect it with our current dead time, but good S_{c-} signals nevertheless could be obtained.

We show in Figs. 4 and 5 a series of 2D ELDOR S_{c-} and S_{c+} spectra (and simulations) over a range of mixing times, T_m, for the 16PC/POPC system. A typical series of COSY and ELDOR S_{c-} experiments (and simulations) for

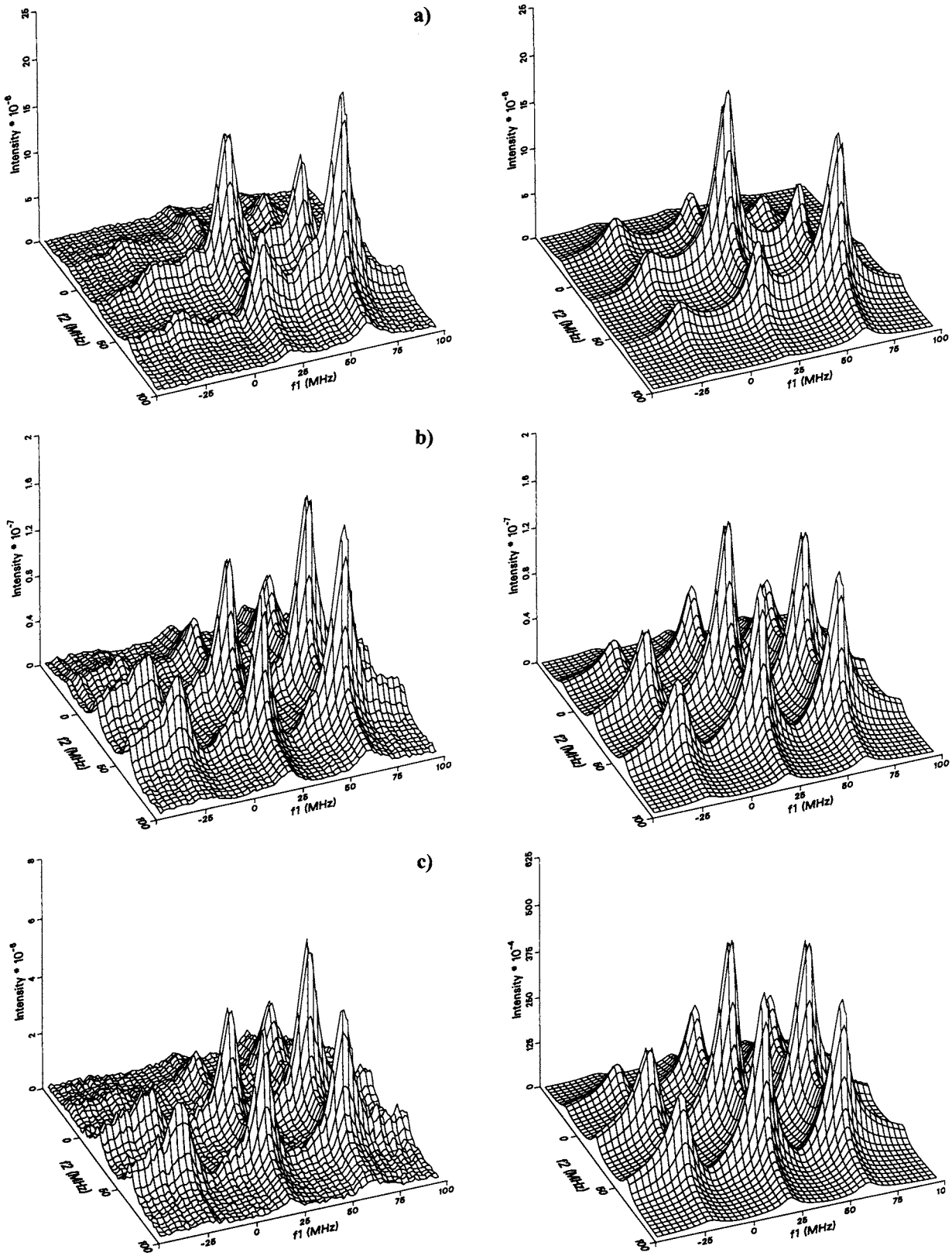

FIGURE 5 2D ELDOR experiments (*left side*) and simulations (*right side*) for 16PC/POPC at 45°C as a function of mixing time, T_m. (*a*) 200 ns; (*b*) 600 ns; and (*c*) 1200 ns. The S_{c+} signal is shown.

CSL at 45°C and 65°C are shown in Figs. 6 and 7. The auto peaks are shown along the positive diagonal in the S_{c+} representation and along the negative diagonal (f_1 reversed) in S_{c-}. The principal difference between the two is that the contributions from inhomogeneous broadening are canceled in the S_{c-} signal due to the echo-like refo-

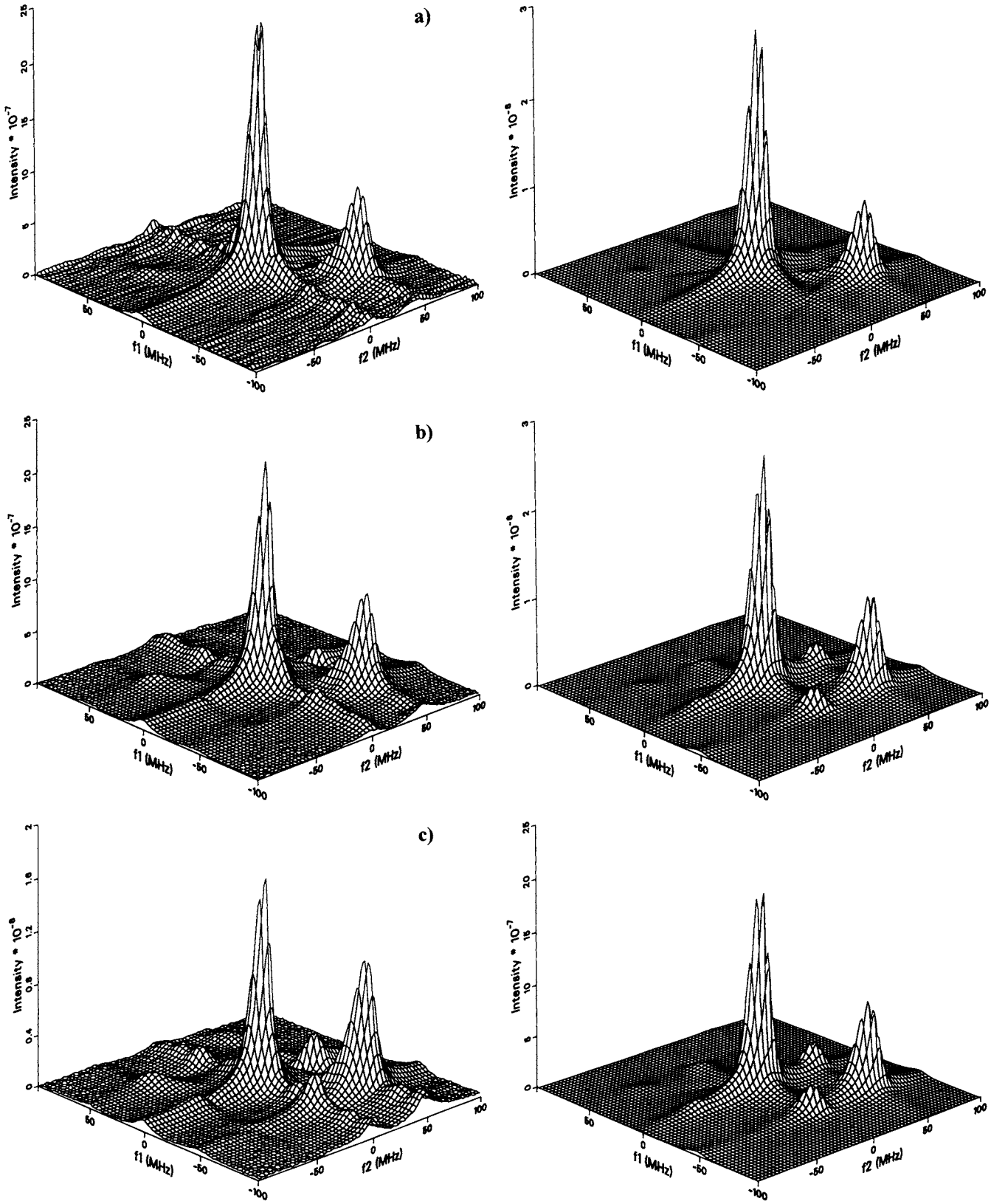

FIGURE 6 2D ELDOR and COSY experiments (*left side*) and simulations (*right side*) for CSL/POPC at 45°C as a function of the mixing time, T_m. (*a*) COSY; (*b*) 110 ns; (*c*) 160 ns; (*d*) 400 ns; and (*e*) 1000 ns. The S_{c-} signal is shown.

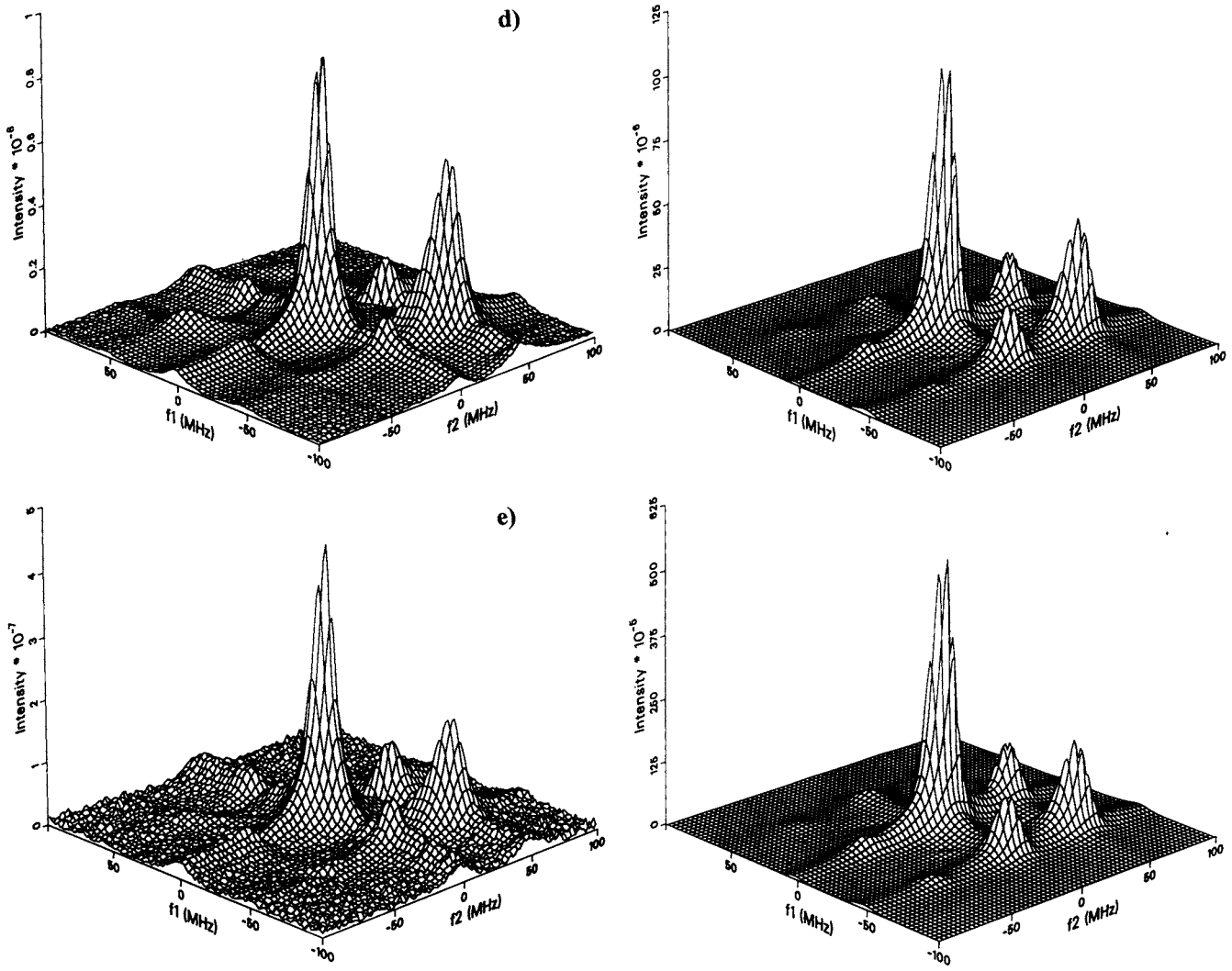

FIGURE 6 (*Continued*)

cussing. This leads to a higher intensity of the S_{c-} signal and subtle differences in peak shapes. For example the peaks in the S_{c-} are elongated along the diagonal auto peak axis (cf. Figs. 6 and 7), and the auto peaks appear sharper in the S_{c-} versus those of S_{c+} (cf. Figs. 4 and 5). These differences become more prominent as the contribution of inhomogeneous broadening increases.

2D ELDOR also provides information on the operative relaxation mechanisms. The growth of cross-peaks versus mixing time T_m may be observed in Figs. 4 and 5 and in Figs. 6 and 7. This development is reflective of cross-relaxation mechanisms like nuclear flips (W_n), and Heisenberg exchange (ω_{HE}), during this time. It is important to note that the END mechanism that leads to nuclear spin flips is restricted by selection rules to single (nuclear) quantum transitions, and therefore they affect only the single quantum cross peaks ($\Delta m_1 = \pm 1$). However for long mixing times, the END mechanism can contribute to the double quantum peaks ($\Delta m_1 = \pm 2$) by two consecutive single quantum transitions. On the other hand HE contributes, equally to the growth of both the single quantum and the double quantum cross-peaks at all mixing times. The CSL experiments in Figs. 6 and 7 show a virtual absence of double quantum cross peaks at all mixing times, hence Heisenberg exchange is deemed to make a negligible contribution, at that temperature. On the other hand, the 16PC spectra show appreciable double-quantum cross-peaks, especially at the higher temperatures, showing a significant ω_{HE} contribution (e.g., Figs. 4 and 5). Therefore even a simple visual observation can be used to disentangle the relative importance of the relaxation processes.

In a vesicle each bilayer segment has a different orientation of its local director. Consequently, the spectrum from each has slightly different hyperfine and g values, resulting in a broadening of the hyperfine peaks. This MOMD effect leads to an asymmetry in the shape of the peaks, because we have more segments perpendicular to the dc-magnetic field than parallel to it. For example, in Figs. 6 and 7, the outer auto peaks are asymmetrically broadened along the auto peaks, i.e., along the negative diagonal in the S_{c-}. Potentially, the shapes of the cross-peaks in 2D ELDOR can be used to

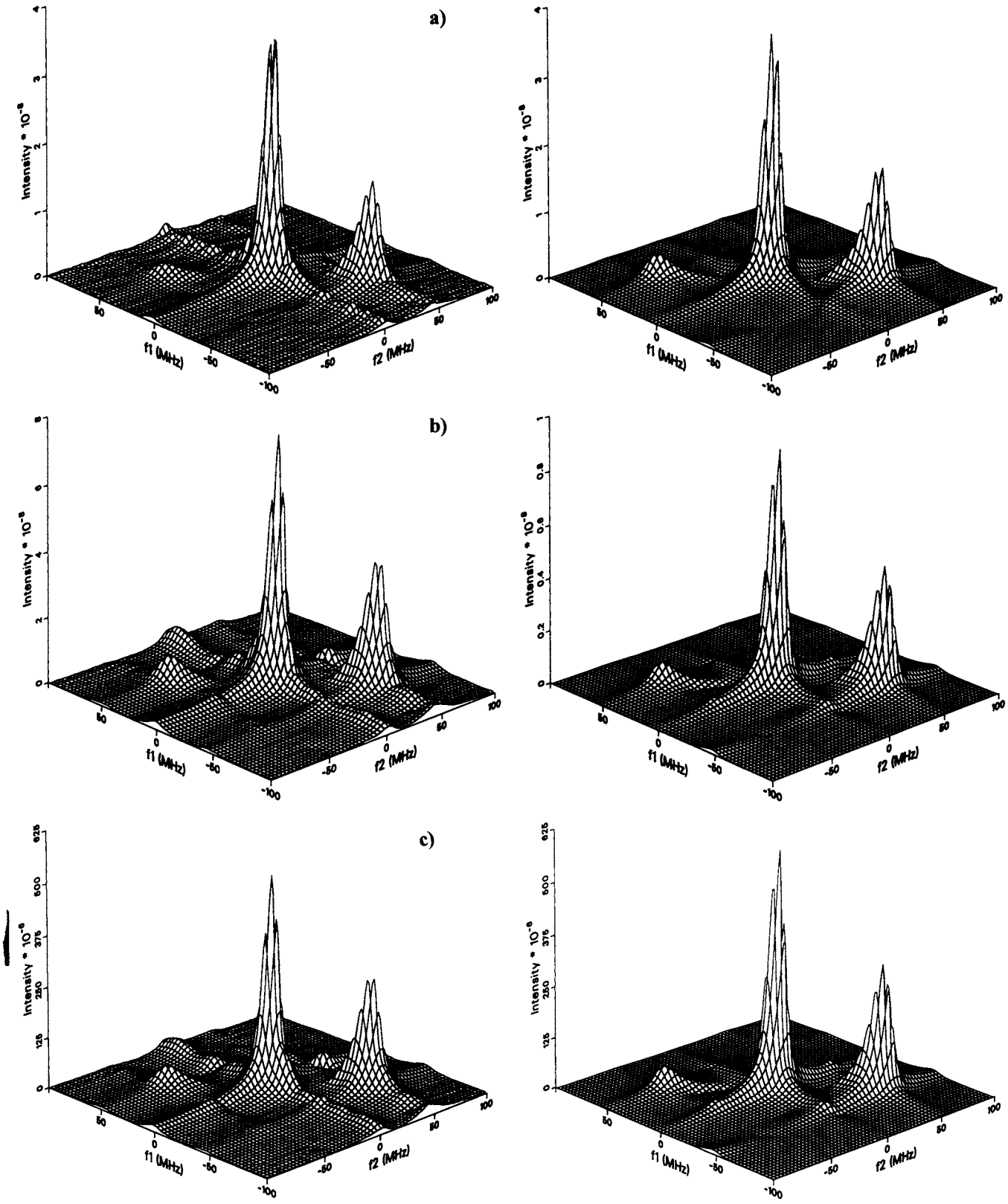

FIGURE 7 2D ELDOR and COSY experiments (*left side*) and simulations (*right side*) for CSL/POPC at 60°C as a function of the mixing time, T_m. (*a*) COSY; (*b*) 78 ns; (*c*) 110 ns; (*d*) 160 ns; (*e*) 400 ns; and (*f*) 1000 ns. The S_{c-} signal is shown.

separate MOMD-type inhomogeneities from other sources of inhomogeneous broadenings. Also CSL shows a greater MOMD effect than 16PC that points to the greater ordering in CSL (i.e., higher potential coefficients).

16PC results

A summary of the optimum parameters obtained from NLLS fits appear in Table 1. These were obtained by simulta-

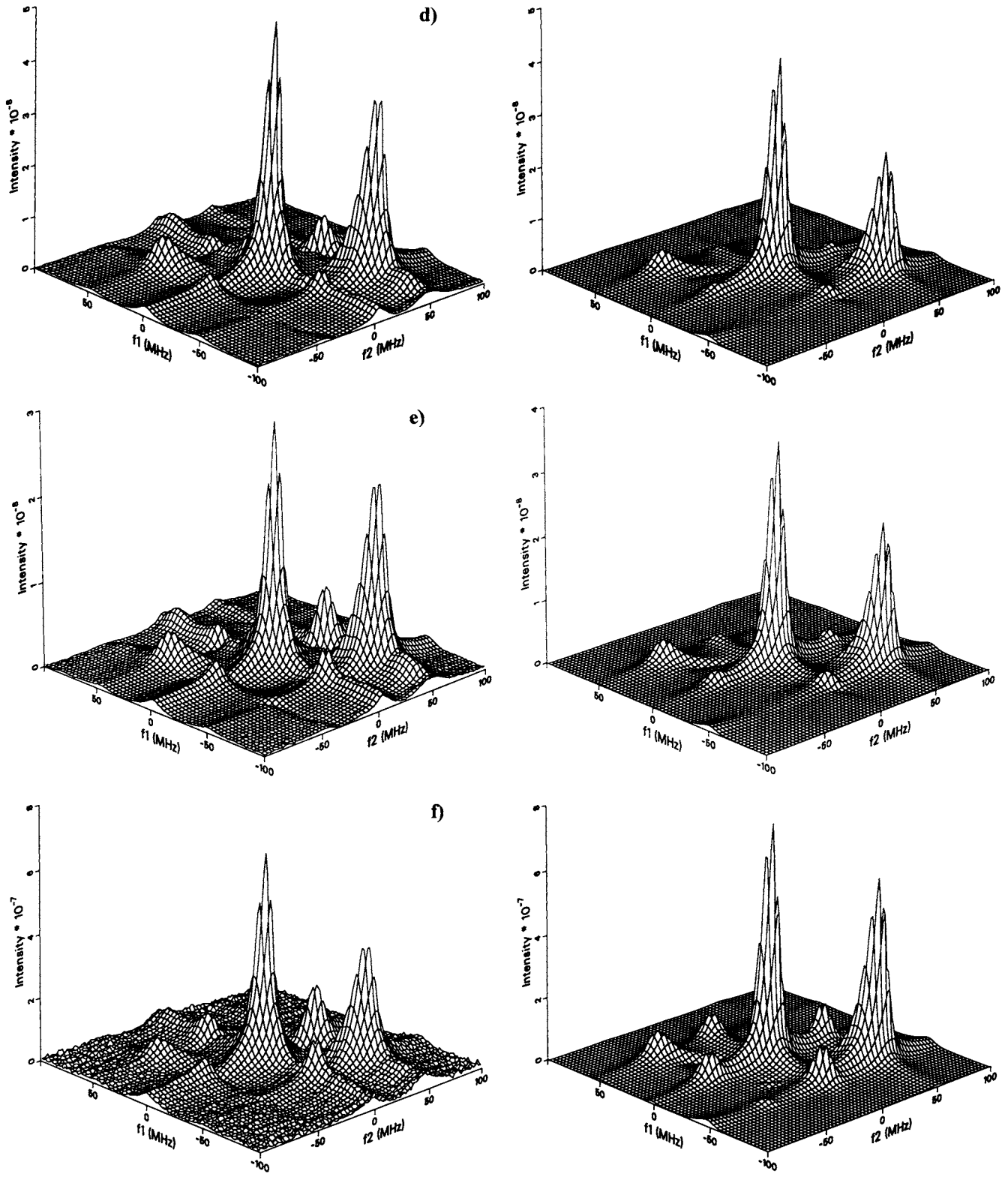

FIGURE 7 (*Continued*)

neously fitting the whole series of mixing times, T_m, as well as the S_{c-} and the S_{c+} spectra. The minimum set of parameters with which we could achieve good fits included the average rotational diffusion coefficient $\bar{R} = (R_\parallel \times R_\perp^2)^{1/3}$, the Heisenberg exchange rate ω_{HE}, the additional homogeneous line-broadening term T_{2e}^{-1}, and the Gaussian inhomogeneous broadening of width Δ. In initial simulations, we found that the results were very insensitive to the rotational anisotropy parameter $N = R_\parallel/R_\perp$. We therefore set $N = 1$, as is customary for fitting cw ESR spectra from aligned samples of this spin

TABLE 1 Rotational and ordering parameters for 16PC

T (°C)	Δ (G)	$\bar{R}$ ($\times 10^9$)s^{-1}	ω_{HE} (μs^{-1})	ϵ_0^2	S	$1/T_{2e}$ (μs^{-1})
25	0.41	0.46	0.0	0.28	0.056	7.99
35	0.25	0.68	0.0	0.21	0.041	16.1
45	0.27	1.62	2.56	0.20	0.038	15.5
55	0.24	1.59	2.32	0.16	0.031	11.7

label (Kar et al., 1985; Shin and Freed, 1989). We also found that because of the low ordering it was sufficient to utilize only one term, ϵ_0^2, in the expansion of the ordering potential. The relative insensitivity to ϵ_2^2 has been found in previous analyses of the cw ESR spectra (Kar et al., 1985; Shin and Freed, 1989).

The Gaussian inhomogeneous broadening is seen to be relatively small (approximately 0.3 G) with little temperature variation. $\bar{R}$, the average rotational diffusion coefficient is seen to increase from 25°C to 45°C (cf. Fig. 8*a*). (There is a slight decrease on going to 55°C. We believe this resulted from a tendency of the sample to lose water through the TPX sample cell at this temperature, which is a deficiency of this type of cell.) The ω_{HE} rate was too small to fit accurately at the lower temperatures but could be measured at 45°C and 55°C. The potential coefficient, ϵ_0^2, shows a monotonic decrease indicating reduced order at higher temperatures (cf. Fig. 8*b*), and this is also true for S, the order parameter which is obtained from ϵ_0^2. A substantial $1/T_{2e}$ was found, but with an unclear temperature dependence.

Shin and Freed (1989) have published results of analyzing cw ESR spectra from oriented samples of 16PC/POPC. However, their samples were at a lower water content (17 weight%) compared with the present study (24 weight%). Our values of $\bar{R}$ are quite similar but a little higher (20–50%) as would be expected for the more fluid higher water content (Shin et al., 1993). Also they show a similar temperature dependence. A comparison of the values of the order parameter S again shows similar trends with temperature, but our 2D ELDOR results on vesicles are about a factor of 2 smaller. Some reduction in S is expected with the increased water content (Shin et al., 1993), but we cannot rule out possible differences between vesicles and ordered multilayers, as monitored by the end chain label. Considering these matters we regard the overall comparison as a favorable one.

The interpretation of the observed homogeneous T_{2e}^{-1} is not entirely clear at present. It may, in part, result from inadequacies in the simulation model, e.g., a needed Lorentzian inhomogeneous broadening component, because for convenience we have assumed a simple Gaussian inhomogeneous broadening component (and it is small). T_{2e}^{-1} is the order of 0.5–1.0 G, rather typical of the extra inhomogeneous broadening from fits of cw ESR spectra. Nevertheless we do wish to call attention to a possible important source of homogeneous broadening. The HE contribution to the width is included automatically in fitting ω_{HE}. However, it is not the only source of cross-relaxation and line broadening resulting from the collision of spin labels. One must also include the electron-electron dipolar (EED) interactions (Nayeem et al., 1989). In fact, in a study of concentration-dependent broadening in 16PC/POPC, both the HE and EED were found to contribute roughly a comparable amount to the concentration-dependent linewidths (Shin et al., 1991). More precisely, one finds that ω_{HE} should be replaced by $\omega_{EX} = \omega_{HE} + \omega_{EED}$ and an additional linewidth contribution to T_{2e}^{-1} from the EED mechanism (not included in the simulations) would be given by $17\omega_{EED}/3$ (Gorcester and Freed, 1988; Nayeem et al., 1989). Thus our results for T_{2e}^{-1} could simply rationalized be as due to $\omega_{EX} \sim \omega_{EED}$ (i.e., $\omega_{EED} > \omega_{HE}$ instead of the expected $\omega_{EED} \sim \omega_{HE}$). Although such matters would require a careful study as a function of spin label concentration before reliable conclusions are to be drawn, there remains a significant point to be made. By means of 2D ELDOR, in which ω_{EX} is obtained from the cross-peak intensities, and the concentration-dependent contributions to T_{2e}^{-1} are also measured, one should be able to separate the ω_{HE} and ω_{EED} terms, a point that has previously been made (Gorcester and Freed, 1988). Finally, in this context we note that we have determined $T_{1e}^{-1} = 2W_e$ and found it to be 1.0 ± 0.2 μs^{-1} over the temperature range studied. Although it would contribute to T_{2e}^{-1}, it is only a small fraction of its observed value.

We now wish to comment on the accuracy and reliability of the NLLS fitting of the 2D ELDOR data. One question in using NLLS fitting is whether the same final parameters are obtained after iterating from different seed values. We have tested this, and we find excellent convergence to better than 0.1% in all fitting parameters, consistent with the nominal

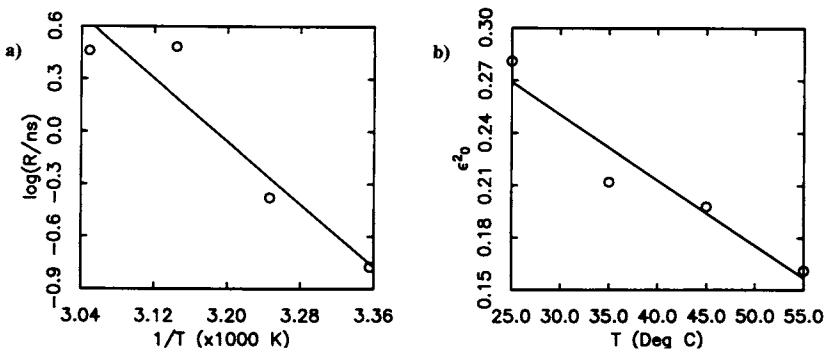

FIGURE 8 The plots of (*a*) log $\bar{R}$ as a function of the inverse of temperature, $1/T$, and (*b*) potential coefficient, ϵ_0^2, as a function of temperature for 16PC/POPC.

TABLE 2 Correlation matrix for 16PC at 45°C

Δ	$\log \bar{R}$	ω_{HE}	ϵ_0^2	$1/T_{2e}$
1.0	−0.1	0.1	−0.1	−0.3
	1.0	0.2	0.2	0.3
		1.0	0.3	−0.7
			1.0	−0.5
				1.0

TABLE 3 Rotational and ordering parameters for CSL

T (°C)	$R_\perp$ $(\times 10^7)s^{-1}$	$R_\parallel$ $(\times 10^9)s^{-1}$	S	ϵ_0^2	ϵ_2^2	ϵ_0^4	Δ (G)
40	2.3	0.5	0.67	4.62	1.42	−0.58	1.2
45	2.6	0.6	0.73	5.25	1.32	−0.54	1.3
50	3.9	1.0	0.71	5.03	1.58	−0.50	1.3
60	5.6	1.7	0.70	4.91	1.38	−0.58	1.2
70	8.5	2.3	0.66	4.52	1.06	−0.74	1.2

error estimates to the fits. Similar estimates of error from analysis of oriented cw ESR spectra are of the order of 1%. Another question is the extent to which the various parameters can be determined independently from 2D ESR spectra. This may be related to the statistical correlation coefficients between variables. A typical correlation matrix (e.g., for 45°C is given in Table 2). We do not find very substantial statistical correlation, except for that between T_{2e}^{-1} and ω_{HE} (which in our experience is not too large). Also, we find these correlations are generally less than those observed from fits of aligned cw ESR spectra.

Of somewhat more concern are the systematic errors, such as trying to fit the data to an imperfect model. For example, in the different context of fitting aligned cw ESR spectra for various tilt angles of the bilayer normal relative to the dc-magnetic field axis, some variation in optimum parameters is typically found when each tilt angle is separately fit (see below). Such discrepancies are probably due to simplifications in our model for ordering and molecular dynamics. In the present case of 2D ELDOR MOMD spectra, we find some systematic discrepancies between the optimum parameters obtained from separately fitting the S_{c+} and the S_{c-} spectra. Although these can be as large as a factor of 2, the temperature-dependent trends of the parameters are nevertheless very similar. The fits from the S_{c-} spectra are found to be very close to those from the combined fits, and these S_{c-} fits are regarded as the more reliable because of their much better signal-to-noise ratio and better resolution (such as to differences in inhomogeneous broadenings) than the S_{c+} signals.

Possible limitations in our model include non-Gaussian contributions to the inhomogeneous broadening, as we have already noted; an unusual variation of the T_{2e}^{-1} with mixing time, T_m, discussed below; and subtleties in the rotational dynamics such as those which led to anomalies in the rotational contribution to W_n versus the T_{2e} values observed in a 2D-FT-ESR study of a well aligned liquid crystal (Gorcester et al., 1989b).

CSL results

Our studies of the CSL/POPC system benefited from the experience gained from the study of the 16PC/POPC system. These included the use of more mixing times as well as the use of the COSY ESR experiment to serve as the $T_m = 0$ ns ELDOR experiment. On the other hand, the greatly reduced overall rotational rate of the rigid CSL spin label and its substantial ordering significantly increased the computational time for the NLLS fitting. Also, its shorter decay times, due largely to the inhomogeneities induced by the MOMD effect, meant that only the S_{c-} signal could be detected, as the S_{c+} signal effectively decayed during the dead time. But good S_{c-} signals were obtained throughout the full temperature range studied. It was found that the simulated spectra were very sensitive to the average rotational rate $\bar{R}$ and less

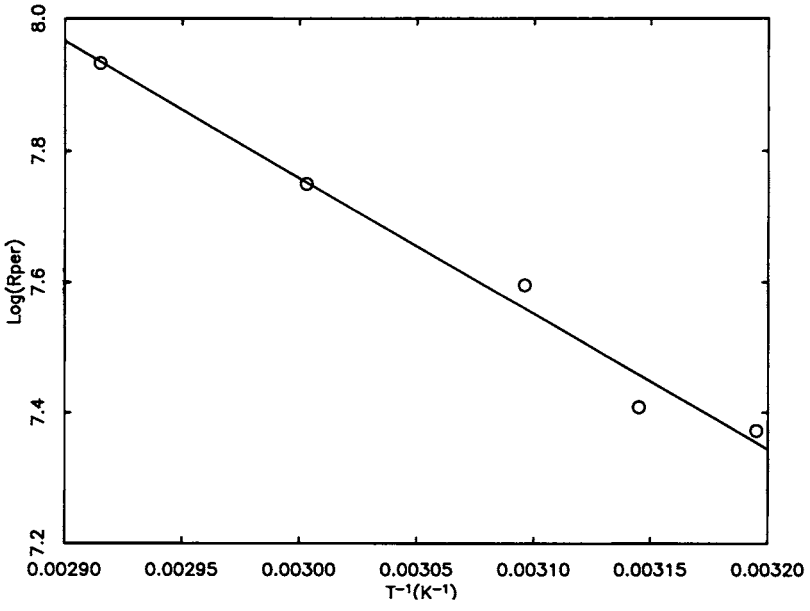

FIGURE 9 The plot of $\log \bar{R}$ as a function of the inverse of temperature, $1/T$ for CSL/POPC.

sensitive to the anisotropy parameter N. Also the potential coefficients, ϵ_0^2 and ϵ_2^2, were more significant than ϵ_0^4. Nevertheless, they all could be fit reliably. However, we found that ω_{HE} was negligible within our experimental error (except perhaps at higher temperatures), and it was not necessary to employ a non-zero T_{2e}^{-1} to obtain good fits. The ordering and diffusion parameters obtained by simulations using the NLLS procedure for results at five temperatures (and 5–6 mixing times) are presented in Table 3. Some experimental and simulated spectra are shown in Figs. 6 and 7.

The rotational diffusion rates decrease with temperature as expected. We plot $\log R_\perp$ versus $1/T$ in Fig. 9. This yields an activation energy for $R_\perp$ of 9.49 kcal·mol^{-1}. The values found for $R_\perp$ compare very well with work of Ge and Freed (1993), using a cw ESR technique and aligned samples. For example they obtained the values of $R_\perp$ to be $3.9 \times 10^7\ s^{-1}$ at 43°C and $5.7 \times 10^7 s^{-1}$ at 59°C. These compare favorably with our results of $2.6 \times 10^7 s^{-1}$ at 45°C and $5.6 \times 10^7 s^{-1}$ at 60°C.

The values of S obtained by our 2D experiments were found to be consistently greater, compared with results of Ge and Freed (1993), from cw ESR. Previous results for S were 0.47 and 0.46 at 43°C and 59°C, respectively, compared with our values of 0.73 and 0.70 at 45°C and 60°C, respectively. This discrepancy can be partially explained in the following way. In fitting cw ESR spectra from aligned samples for the bilayer axis both parallel and perpendicular to the dc-magnetic field, it is the parallel orientations that are found to weigh more in such simulations. However, we do find that aligned CSL samples with the bilayer axis perpendicular to the magnetic field are better fit with S about 15–20% higher. It is these perpendicular (and generally nonparallel) orientations that are weighted much more heavily in the averaging leading to a MOMD spectrum. (This effect is much less important for 16PC, because its ordering is much less.)

Additionally we find that the more well aligned a sample is, the higher are the order parameters obtained from simulations. Small imperfections in alignment of samples can reduce their apparent values of S. Finally, we do note that there could be differences in the ordering of sterol molecules like CSL in vesicles as compared with oriented multilayers, but further work would be required to distinguish this from other factors.

We now turn to the accuracy and reliability of fitting the 2D ELDOR and COSY data for CSL. The NLLS error estimates indicate convergence to at least as good as 0.5% in the main fitting parameters, whereas similar estimates from fitting the oriented cw ESR spectra indicate errors that are an order of magnitude greater. We also have considered

TABLE 4 Correlation matrix of parameters for CSL at 70°C

Δ	$\log\bar{R}$	$\log N$	ϵ_0^2	ϵ_2^2	ϵ_0^4
1.0	−0.1	0.1	−0.1	−0.1	0.0
	1.0	−0.1	−0.4	−0.4	0.1
		1.0	−0.5	−0.8	−0.7
			1.0	0.7	0.5
				1.0	0.5
					1.0

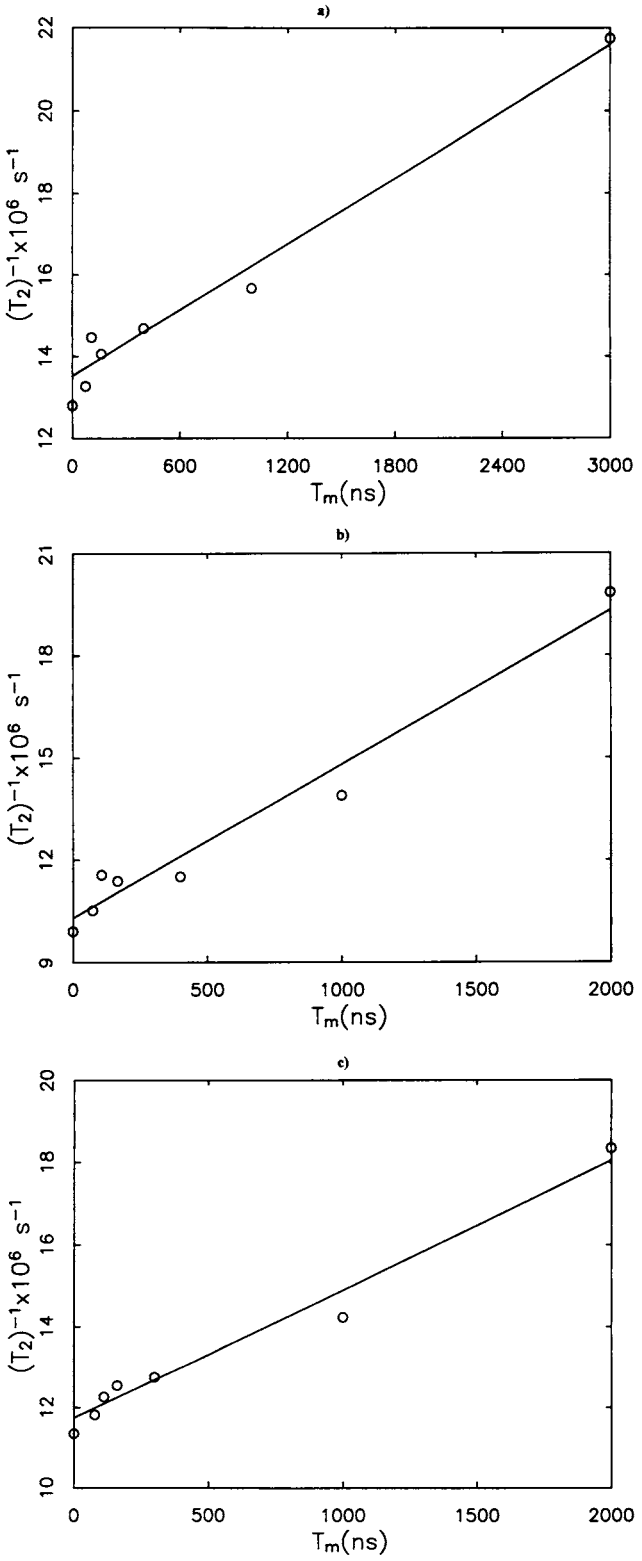

FIGURE 10 The plot of apparent homogeneous linewidths, T_2 values as a function of the mixing time, T_m, for CSL/POPC at three different temperatures: (*a*) 50°C; (*b*) 60°C; and (*c*) 70°C.

the statistical correlation coefficients between the variables, and a typical correlation matrix (e.g., for 70°C) is given in Table 4. As expected, there is some statistical correlation in fitting the potential coefficients ϵ_0^2, ϵ_2^2, and ϵ_0^4, but this did not interfere very significantly with their fits. Also, some correlation between log N and these potential coefficients was found. We believe that this correlation is a source of reduced accuracy in N (versus $\bar{R}$) referred to above. We find significantly greater correlation coefficients for fits from aligned cw-ESR spectra from CSL.

We now wish to describe an unusual and significant observation. It is possible to obtain the homogeneous T_2 values across the inhomogeneously broadened spectra from COSY-ESR spectra. One must perform an axis transformation on the S_{c-} signal (Gamliel and Freed, 1990) by replacing $t_2 \rightarrow t_1 + t_2$, which yields the equivalent of the SECSY-ESR spectra. After Fourier transforming with respect to the new t_2 variable, the exponential decays in t_1 lead to the homogeneous T_2 values. The equivalent axis transformation on the S_{c-} 2D ELDOR signal enables one to extract the analogous T_2 values from the auto peaks. We find that these "apparent" T_2 values are increasing linearly with the mixing time, T_m. This is illustrated in Fig. 10 for the central auto peak at three different temperatures. This effect seems to be increasing with increasing temperature. A similar trend, although less pronounced, was found for the higher frequency auto peak. (The intensity, hence the signal-to-noise ratio, of the lowest frequency auto peak was too low over the entire temperature range to conduct this analysis.) An attempt was made to extract such an effect from the 16PC/POPC data (which included the SECSY ESR spectrum), but its limited accuracy and the few mixing times studied precluded such an analysis.

Observations similar to these were actually made by solid-state 2D ELDOR studies on malonic acid single crystals (Lee et al., 1993). These results were rationalized as possibly due to modulation of the amplitude and/or orientation of the proton hf and g-tensors by low frequency phonon modes. We suggest that the present observations are due to fluctuations in the direction of alignment of the lipid (and sterol) molecules in the vesicle, i.e., collective director fluctuations. This mechanism is known to make a significant contribution to spin relaxation in nuclear magnetic resonance studies of membranes (Mayer et al., 1988; Watnick et al., 1987). However, they are too slow to contribute to the ESR T_1 and T_2 values (Polnaszek and Freed, 1975). In our present interpretation, one is observing the "real-time" motion of a spin label with the director orientation Ψ slowly changing to a new orientation Ψ' or else the label is diffusing into a region with director orientation Ψ'. Because this entails a slight change in the ESR resonant frequency, an "exchange cross-peak" appears. But because there is a continuum of values Ψ' that however are close to Ψ in value, the cross-peaks appear as an apparent increase in the broadening of the auto peaks versus T_m. Such a real-time observation of the effects of director fluctuations should enable their accurate study by 2D ELDOR.

CONCLUSIONS

1. The 2D-FT-ESR experiments of 2D ELDOR, COSY ESR, and SECSY ESR can be performed successfully on membrane vesicles containing labeled lipids and labeled sterols. This can greatly enhance the range and variety of membrane samples for which accurate ESR studies can be performed.
2. These experiments (especially in the 3D format obtained as a function of mixing time, T_m) in conjunction with the nonlinear least squares spectral analysis, lead to precise determination of molecular dynamic properties including the rotational tensor and spin exchange rates, as well as the molecular orientational ordering. The precision obtained by these methods applied to vesicle dispersions is better than that of comparable studies on aligned membrane multilayers by conventional cw ESR methods. The results on rotational diffusion rates obtained by both methods compare favorably for similar (but not identical) types of sample composition, although some differences in ordering are found.
3. Because both approaches, namely 2D-FT-ESR and cw ESR, fitted by NLLS spectral simulations involve subtle differences in detail and analysis, a study of dynamic molecular structure of membrane vesicles versus lamellar multilayers would be performed best by comparing 2D-FT-ESR results on both types of samples.
4. There is some indication that collective dynamics, such as director fluctuations in membrane vesicles, can be studied in "real time" by 2D ELDOR.

This work was supported by National Institutes of Health grants GM25862 and RR07126 and National Science Foundation grants CHE9312167 and DMR 9210638. Computations were performed at the Cornell National Supercomputer Facility, Ithaca, NY.

REFERENCES

Crepeau, R. H., S. Rananavare, and J. H. Freed. 1987. Automated least squares fitting of slow motional ESR spectra. *Abstracts of the 10th International EPR Symposium, Rocky Mountain Conference, Denver, CO.*

Crepeau, R. H., A. Dulcic, J. Gorcester, T. R. Saarinen, and J. H. Freed. 1989. Composite pulses in time domain ESR. *J. Magn. Reson.* 84:184–190.

Devaux, P. F., and M. Seignenret. 1985. Specificity of lipid-protein interactions as determined by spectroscopic techniques. *Biochim. Biophys. Acta.* 822:63–125.

Ferrarini, A., P.-L. Nordio, G. J. Moro, R. H. Crepeau, and J. H. Freed. 1989. A theoretical model of phospholipid dynamics in membranes. *J. Chem. Phys.* 91:5707–5721.

Freed, J. H. 1987. Molecular rotational dynamics in isotropic and oriented fluids studied by ESR. *In* Rotational Dynamics of Small and Macromolecules in Liquids. T. Dorfmuller and R. Pecora, editors. Springer-Verlag, Germany 89–142.

Gamliel, D., and J. H. Freed. 1990. Theory of two-dimensional ESR with nuclear modulation. *J. Magn. Reson.* 89:60–93.

Ge, M., and J. H. Freed. 1993. An ESR study of interactions between gramicidin A′ and phosphatidylcholine bilayers. *Biophys. J.* 65: 2106–2123.

Gorcester, J., and J. H. Freed. 1988. Two-dimensional Fourier transform ESR correlation spectroscopy. *J. Chem. Phys.* 88:4678–4693.

Gorcester, J., G. L. Millhauser, and J. H. Freed. 1989a. Two dimensional

and Fourier transform ESR. *In* Advanced EPR Applications in Biology and Biochemistry. A. J. Hoff, editor. Elsevier, Amsterdam. 177–242.

Gorcester, J., S. B. Rananavare, and J. H. Freed. 1989b. Two dimensional electron spin echo study of solute dynamics in smectics. *J. Chem. Phys.* 90:5764–5786.

Gorcester, J., G. L. Millhauser, and J. H. Freed. 1990. Two dimensional electron-spin resonance. *In* Advances in Pulsed and Continuous Wave Electron Spin Resonance. L. Kevan and M. Bowman, editors. Wiley, New York. 119–194.

Hornak, J. P., and J. H. Freed. 1986. Spectral rotation in pulsed ESR spectroscopy. *J. Magn. Reson.* 67:501–518.

Hubbell, W. L., and H. M. McConnell. 1971. Molecular motion in spin-labeled phospholipids and membranes. *J. Am. Chem. Soc.* 93:314–320.

Kar, L., E. Ney-Igner, and J. H. Freed. 1985. Electron spin resonance and electron-spin echo study of oriented multilayers L_α-phosphatidylcholine water systems. *Biophys. J.* 48:569–595.

Lee, S., B. R. Patyal, and J. H. Freed. 1993. A two-dimensional Fourier transform electron-spin resonance (ESR) study of nuclear modulation and spin relaxation in irradiated malonic acid. *J. Chem. Phys.* 98: 3665–3689.

Marsh, D. 1985. ESR probes for structure and dynamics of membranes. *In* Spectroscopy and Dynamics of Molecular and Biological Systems. P. M. Bayley and R. E. Dale, editors. Academic, Press, London. 209–238.

Mayer, C., K. Muller, K. Weisz, and G. Kothe. 1988. Deuteron NMR relaxation studies of phospholipid membranes. *Liq. Crys.* 3:797–806.

Meirovitch, E., A. Nayeem, and J. H. Freed. 1984. An analysis of protein-lipid interactions based on model simulations of ESR spectra. *J. Phys. Chem.* 88:3454–3465.

More, J. J. 1977. The Levenberg-Marquardt algorithm: implementation and theory. *In* Numerical Analysis; Lecture Notes in Mathematics. G. A. Watson, editor. 630:105–116.

Nayeem, A., S. R. Rananavare, V. S. S. Sastry, and J. H. Freed. 1989. Heisenberg spin exchange and molecular diffusion in liquid crystals. *J. Chem. Phys.* 91:6887–6905.

Patyal, B. R., R. H. Crepeau, D. Gamliel, and J. H. Freed. 1990. Two dimensional Fourier transform ESR in the slow motional and rigid limits: SECSY-ESR. *Chem. Phys. Lett.* 175:445–452.

Polnaszek, C. F., and J. H. Freed. 1975. ESR studies of anisotropic ordering, spin relaxation, and slow tumbling in liquid crystalline solvents. *J. Phys. Chem.* 79:2283–2306.

Popp, C. A., and J. S. Hyde. 1981. Effects of oxygen on EPR spectra of nitroxide spin-label probes of model membranes. *J. Magn. Reson.* 43: 249–258.

Schneider, D. J., and J. H. Freed. 1989. Calculating slow motional magnetic resonance spectra: a user's guide. *In* Biological Magnetic Resonance. Vol. 8. L. J. Berliner and J. Reuben, editors. Plenum Publishing Corp., New York. 1–76.

Shin, Y.-K., and J. H. Freed. 1989. Dynamic imaging of lateral diffusion by electron spin resonance and study of rotational dynamics in model membranes: effect of cholesterol. *Biophys. J.* 55:537–550.

Shin, Y.-K., U. Ewert, D. E. Budil, and J. H. Freed. 1991. Microscopic and macroscopic diffusion in model membranes by ESR spectral-spatial Imaging. *Biophys. J.* 59:950–957.

Shin, Y.-K., D. E. Budil, and J. H. Freed. 1993. Thermodynamics and dynamics of phosphatidylcholine-cholesterol mixed model membranes in the liquid crystalline state: effects of water. *Biophys. J.* 65:1283–1294.

Tanaka, H., and J. H. Freed. 1984. Electron spin resonance studies of ordering and rotational diffusion in oriented phosphatidylcholine multilayers: evidence for a new chain-ordering transition. *J. Phys. Chem.* 88: 6633–6644.

Tanaka, H., and J. H. Freed. 1985. Electron spin resonance studies of lipid-gramicidin interactions utilizing oriented multilayers. *J. Phys. Chem.* 89: 350–360.

Watnick, P., D. Phoebe, A. Nayeem, and S. I. Chan. 1987. Cooperative lengths and elastic constants in lipid bilayers: The chlorophyll a/ dimyristollecithin system. *J. Chem. Phys.* 86:5789–5800.